6372–6383 *Nucleic Acids Research, 2005, Vol. 33, No. 19*
doi:10.1093/nar/gki942

Shared RNA-binding sites for interacting members of the *Drosophila* ELAV family of neuronal proteins

Claudia D. Borgeson[1] and Marie-Laure Samson[1,2,*]

[1]Department of Biochemistry and Molecular Biology, University of Nebraska Medical Center, Omaha, NE 68198-4525, USA and [2]Laboratoire Signalisation, Développement et Cancer, UMRC8080, CNRS, Université Paris Sud, Bâtiment 442 bis, 91405 Orsay Cedex, France

Received September 6, 2005; Revised and Accepted October 17, 2005 DDBJ/EMBL/GenBank accession nos.[+]

ABSTRACT

The product of the *Drosophila embryonic lethal abnormal visual system* is a conserved protein (ELAV) necessary for normal neuronal differentiation and maintenance. It possesses three RNA-binding domains and is involved in the regulation of RNA metabolism. The long *elav* 3′-untranslated region (3′-UTR) is necessary for autoregulation. We used RNA-binding assays and *in vitro* selection to identify the ELAV best binding site in the *elav* 3′-UTR. This site resembles ELAV-binding sites identified previously in heterologous targets, both for its nucleotide sequence and its significant affinity for ELAV (K_d 40 nM). This finding supports our model that *elav* autoregulation depends upon direct interaction between ELAV and *elav* RNA. We narrowed down the best binding site to a 20 nt long sequence $A(U_5)A(U_3)G(U_2)A(U_6)$ in an alternative 3′ exon. We propose and test a model in which the regulated use of this alternative 3′ exon is involved in normal *elav* regulation. Found in NEurons (FNE), another neuronal RNA-binding protein paralogous to ELAV, also binds this site. These observations provide a molecular basis for the *in vivo* interactions reported previously between *elav* and *fne*.

INTRODUCTION

The *Drosophila* gene *embryonic lethal abnormal visual system (elav)* encodes (ELAV) protein that is the founding member of a family of primarily neuronal RNA-binding proteins that exist in all metazoans (1). Proteins from this family contain three RNA recognition motif (RRMs), with a long variable hinge separating RRM2 from RRM3 (1). Proteins with RRMs typically interact with RNA, and act as post-transcriptional regulators. In addition, RRM domains can also serve other functions. For example the RRM of the *Y14* protein, present in complexes at exon junctions, forms heterodimers with the *Mago-nashi* protein, (2,3). RRM–DNA interactions have also been reported (4).

Drosophila ELAV is required for the normal differentiation and maintenance of all neurons, appearing in postmitotic neurons and persisting at all stages of development (1,5). A second member of the family, RBP9 (6), is produced starting at the third larval instar in all neurons, where its function remains unclear. It is also present in the cytoplasm of cystocytes where it is necessary for female fertility (7). The product of the third paralogue, found in neurons (*fne*), is detected shortly after ELAV with the same neuronal specificity, except that FNE appears to be cytoplasmic, while ELAV and neuronal RBP9 are nuclear (8). Over-expression of FNE in neurons has shown that the two paralogues *elav* and *fne* interact (8). In vertebrates, HuR, one of four ELAV orthologues, is ubiquitously expressed (9), while the other three are early markers of neuronal differentiation, and persist in some mature neurons (10). The importance of these proteins for neuronal plasticity is reflected by their accumulation during acquisition of spatial memory in neurons of the hyppocampus (11,12).

ELAV family proteins bind with a distinct preference to U-rich sequences with apparent dissociation constants (K_d) in the 1–100 nM range (9,13–20). Modest poly(A) binding (K_d 146 nM) by the RRM3 of HuD, HuC and HuR (the vertebrate homologues) has also been described (21,22). The crystal structure of RRM–RNA complexes have been determined both for the first two RRMs of HuD (23) and for the two RRMs of the *Drosophila* Sex lethal protein (SXL), which resemble *Drosophila* ELAV (24). The pairs of RRMs of

*To whom correspondence should be addressed. Tel: +33 1 69 15 75 85; Fax: +33 1 69 15 68 03; Email: MLaure.Samson@ibaic.u-psud.fr
Present address:
Claudia D. Borgeson, The Eppley Institute for Research in Cancer and Allied Diseases, University of Nebraska Medical Center, Box 986805, Omaha, NE 69198-6805, USA

[+]DQ004736, DQ243913 and DQ243914

HuD and SXL proteins fold very similarly and are associated with a single RNA molecule. Each RRM constitutes a binding pocket for distinct regions of the RNA, without base pairing (25). Conserved residues in the RRM, in particular in the two characteristic ribonucleoprotein (RNP) motifs, make direct nucleotide contacts relying upon specific recognition of the bases (23). Individual RRMs can still interact with the RNA target, but with decreased efficiency (19,20,26,27). Comparison of known RNA–RRM structures indicates that although the proteins adopt similar tertiary structures, specific RNA molecules adopt diverse conformations and orientations (23).

Functions in RNA stabilization, export and translation have been assigned to the vertebrate Hu proteins [for instance (28–33)], while RBP9 has been proposed to destabilize RNA (7). *Drosophila* ELAV, through direct binding in the vicinity of polyadenylation sites located in alternative introns, promotes the accumulation of alternative forms of mRNAs encoding alternative protein forms specific to or enriched in neurons (14,16,34,35). In addition, we have shown that *elav* autoregulates through a mechanism requiring its 3′-untranslated region (3′-UTR) (36). Owing to this autoregulation, the level of ELAV protein in neurons is independent of *elav* gene dosage. Versions of the *elav* gene with a truncated 3′-UTR do not autoregulate, and flies carrying two copies die, except for a few escapers (36).

In order to obtain further insight into the mechanism of *elav* autoregulation, the identification of the ELAV best binding site on the 3′-UTR of its own RNA was crucial. For this purpose, we used a customized version of *in vitro* selection whose merit was to identify actual sequences, as opposed to defining artificial consensus sequences. We mapped the site, a U-rich sequence, to an alternative 3′ exon retained in a non-coding mRNA that otherwise shares the upstream non-coding exon of the functional *elav* mRNA. This binding site differs from the ELAV-binding sites mapped previously in the introns of *nrg* and *ewg* targets, since it is exonic and at a distance from polyadenylation sites. However, it shares with the *ewg* and *nrg* sites a similarly high U content and a low K_d (40 nM) for ELAV association. This suggests a dual molecular function for ELAV, respectively for autoregulation and the regulation of the metabolism of other RNAs. We also found that individual RRMs bind specific targets with different relative specificities, suggesting that different pairs of RRMs may be responsible for specific-target recognition. Finally, we found that FNE can bind to the same targets as ELAV, providing a possible molecular basis for previously described *elav*/*fne* interactions *in vivo*.

MATERIALS AND METHODS

Fusion proteins

The 483 amino acid long ELAV contains an N-terminal Q-A rich region (amino acids 26–126) and three RRMs. The 356 amino acid long FNE protein is very similar, with a 24 amino acid long N-terminus upstream of the three RRMs (8). The glutathione *S*-transferase (GST) gene fusion system (Pharmacia Biotech) was used to produce fusion proteins. Open reading frames (ORFs), either as restriction fragments or as PCR products, were cloned in-frame into pGEX-2T. After sequencing of the cloning junctions and of the cloned PCR products, the plasmids were used to produce proteins according to the manufacturer's instructions: GST-ELAV (residues 76–483), GST-RRM1 (residues 76–242), GST-RRM2 (residues 229–324), GST-RRM3 (residues 364–483) and GST-FNE2 (residues 15–356), the latter being poorly soluble.

Construction of the *elav* 3′-UTR RNA pool

A library was constructed by sonication of a 7.5 kb BamHI (p7.5BB) genomic clone which included the *elav* stop codon and the complete 3′-UTR, containing sequences necessary for *elav* autoregulation (36). The 100 bp fragments were gel purified and ligated into a modified pUC18 vector whose HindIII–EcoRI polylinker fragment had been replaced by a new sequence introducing an EcoRV site for cloning, restriction sites for insert manipulation and a T7 promotor. The new sequence was generated by the annealing of two 61mer oligonucleotides AGCTAATACGACTCACTATAGGGAGCTCAGAATAAACGCTGATATCGACATGAGGCCCGG (Selex5) and AATTCCGGGCCTCATGTCGATATCAGCGTTTATTCTGAGCTCCCTATAGTGAGTCGTATTA (Selex6).

Independent clones (1500) were obtained after transformation, referred to as the original library (OL). The colonies on the transformation plates were recovered in Luria–Bertani, and the cell suspension was used to inoculate two 250 ml cultures. The cultures were used to purify OL DNA. Characterization of the library was performed by testing 24 independent clones: 18 of the clones contained an insert ~100 nt long, 2 contained a double insert and 3 none. Sequencing of three clones revealed 73, 93 and 105 nt long inserts corresponding to different regions of the 3′-UTR. In addition, Southern blot analysis of p7.5BB with a probe made from the OL DNA showed that the library was representative (Results).

An aliquot of OL DNA was PCR amplified using the 23mer CGAATTCCGGGCCTCATGTCGAT (Selex3) and the 48mer GCCAAGCTTAATACGACTCACTATAGGGAGCTCAGAATAAACGCTGAT (Selex4). The amplified DNA (up to 4 µg DNA in 100 µl) was transcribed by T7 RNA polymerase in 40 mM Tris, pH 7.9, 6 mM $MgCl_2$, 2 mM spermidine, 10 mM DTT, 0.5 mM each G-, A-, U-, CTP, 10^{-3} mM [α-^{32}P]CTP 800 Ci/mmol (Amersham), 100 U RNasin (Promega) and 25 U T7 RNA polymerase (Promega). After 1 h incubation at 37°C, the reaction was treated at 37°C for 15′ with 5 U RQ1 DNase (Promega). Subsequent purification on a 6% acrylamide, 7M urea gel (elution buffer: 2 mM EDTA and 500 mM ammonium acetate) yielded the first pool of RNAs for partitioning. In these labelling conditions, *n* d.p.m./µl of purified labelled RNA corresponds to a µM concentration of [$n \times 2.8\ 10^{-4}$/number of C residues in the RNA].

In vitro selection

We performed the partitioning between ELAV-bound and -unbound RNAs using conditions that gave 1–5% RNA-binding per cycle. The GST-ELAV concentration allowing the desired percentage of binding was determined before each cycle as follows: small-scale binding reactions (10 µl) were set up between GST-ELAV (3 nM to 3.1 µM by serial 2-fold dilutions) and a pool of heat-denatured RNAs (25 000 d.p.m.) in 110 mM NaCl, 20 mM Tris–HCl, pH 7.5, 2.5 mM

$MgCl_2$, 2.5 mM KCl, 8 mM NaH_2PO_4, 2 mM KH_2PO_4, 3 mM DTT, 100 ng/µl tRNA, 0.6 U/µl RNasin (Promega) and 1% glycerol. After a 15 min incubation at 37°C, the reactions were filtered on pre-wet nitrocellulose (Millipore HAWP 02500) in a sampling manifold (Millipore XX2702550) as in (37). The percentage of bound RNA was calculated as follows: radioactivity retained on the filter ×100/radioactivity (recovered in the flow through + retained on the filter).

The reaction allowing the desired percentage binding was scaled up (100–200 µl) for partitioning and the ELAV-bound RNA was purified on nitrocellulose. The RNA was recovered by incubation of the cut filter 30 min at room temperature with 200 µl of 10 M urea, 400 µl phenol, pH 7.6 and 200 µl chloroform, recovery and re-extraction of the aqueous phase with phenol/chloroform before ethanol precipitation. The purified sample was annealed with 1.3 µg of Selex3 oligonucleotide in 40 µl of 20 mM Tris, pH 7.5 and 10 mM $MgCl_2$. Reverse transcription was performed with Superscript RNase H^- reverse transcriptase (Life Technologies) according to the manufacturer's instructions, in a 100 µl reaction volume, of which 5% was removed before the addition of RT, as a control.

Optimal conditions for PCR amplification of the cDNA were determined at each cycle as follows: four amplification reactions were set up in 50 µl, using as substrate (i) 5 µl of the cDNA obtained by reverse transcription, (ii) 5 µl of the control reaction without RT, (iii) 1 ng OL DNA, and (iv) no substrate, with 0.4 µg Selex3, 1 µg Selex4, 50 nM each dNTP in 50 mM KCl, 10 mM Tris–HCl, pH9, 0.1% Triton X-100 and 1.5 mM $MgCl_2$. Each reaction was divided among four 12.5 µl tubes, heated to 95°C for 5 min before addition of 0.6 U *Taq* DNA polymerase (Promega) at 80°C, and amplification was performed by incubation for 1 min at 94°C, 1 min at 55°C, 1 min at 72°C for n cycles ($n = 8$, 10, 12 and 14), followed by 7 min at 72°C. The cycle number giving optimal amplification of the cDNA was used for a scaled up experiment. The amplification products were phenol-chloroform extracted before ethanol precipitation and resuspension in 100 µl H_2O. Subsequent T7 polymerase transcription and partitioning cycles were performed in similar conditions.

Shift assays and binding curves

Labelled RNA was synthesized as above in a 10 µl reaction, except that [α-^{32}P]UTP 800 Ci/mmol was used at a concentration 2.5×10^{-4} mM. In these labelling conditions, n d.p.m./µl of purified labelled RNA corresponds to a mM concentration of [$n \times 1.125\ 10^{-3}$/number of U residues in the RNA]. The DNA flanked by Selex3 and Selex4 sequences (template concentration: 60 nM for PCR products or 2 nM for HindIII plus EcoRI digested plasmid DNA) was transcribed with T7 polymerase and gel purified as needed on urea gels, followed by elution in 1% SDS, 25 µg/ml tRNA and 500 mM ammonium acetate. For shift assays, labelled RNA (1000–2000 d.p.m.) in 5 µl of 100 mM NaCl, 20 mM Tris–HCl, pH 7.5 and 1 µg tRNA, was heated for 3 min at 85°C, and cooled on ice. Binding reactions (10 µl) between heat-denatured RNA and proteins (as specified in each experiment) were in 110 mM NaCl, 20 mM Tris–HCl, pH 7.5, 2.5 mM $MgCl_2$, 2.5 mM KCl, 8 mM Na_2HPO_4, 2 mM KH_2PO_4, 0.1 µg/µl tRNA, 3 mM DTT, 0.6 U/µl RNasin (Promega) and 1% glycerol at 37°C for 15 min. Glycerol dye (1 µl of 50% glycerol and 5% bromophenol blue) was added to the reactions before analysis on a 0.75 cm thick acrylamide/bis (80:1) gel run at 120 V in 0.5× TBE, and dried before autoradiography.

Binding curves were established by nitrocellulose filtration as above, except that GST-ELAV concentrations were between 640 and 0.625 nM (2-fold dilutions) and 5000 d.p.m. of heat-denatured labelled RNAs were used.

Sequence data

After purification with Wizard PCR Preps DNA purification system (Promega), aliquots of the PCR amplified cDNA deriving from selected RNAs were cloned into pGEM-T (Promega) according to the manufacturer's intructions. *elav* cDNA clone RE58603 from the Berkeley *Drosophila* Genome Project (38) was obtained from Invitrogen Life Technologies, and additional partial cDNAs were obtained as in (8). Sequencing was performed on Applied Biosytems and Li-Cor sequencers by the University of Nebraska Medical Center/Eppley Molecular Biology core Facility or MWG Biotech. Sequence analysis was performed with the GCG Wisconsin Package (Version 10.2; Genetics Computer Group, Madison, WI). The LD33076 sequence was obtained from GenBank under accession number AY051822. We deposited the RE58603, RE14370 and cDNA3h sequences under accession numbers DQ004736, DQ243914 and DQ243913.

Generation of specific target RNAs

PCR amplification was performed with pairs of oligonucleotides framing the ELAV best binding sites respectively in the *elav* 3′-UTR (S11F, CTTGATGAAAATTTTAGCATC; S11R, GAGAGGGAAACAAGTATAG; template, cloned *elav* 3′-UTR) and in a *neuroglian* intron (nrg1, CATATTTTGTGTTCCTTG; nrg2, GTGTTTATTTTACGTGTTTAG; template, genomic DNA). Clones of the PCR products in pGEM-T were modified (restriction digest followed by T4 polymerase repair before circularization) to reduce the region between the start of transcription and the insert, and sequenced. T7 transcripts were produced and purified as above after linearization with NotI or RsaI.

Homoribopolymer binding assay

Proteins were incubated in 500 µl binding buffer 20 mM Tris–HCl, pH 7.5, 2.5 mM $MgCl_2$, 0.5% Triton X100, 0.1 M NaCl for 10 min at 4°C with homoribopolymers bound to resins (Sigma P 1908, P 5643, D 8563 and D 9827). The resins were washed three times for 10 min at 4°C in binding buffer, resuspended in 2× Laemmli loading buffer, incubated for 5 min at 90°C before SDS–PAGE, followed by Coomassie blue staining. Alternatively (for individual RRMs), the detection was performed with a polyclonal antibody detecting the GST moiety of the GST fusions proteins (anti-GST:FNE antibody).

Northern blot analysis and RT–PCR

Northern blot analysis was performed as in (8) using single-stranded RNA (ssRNA) antisense probes. For RT–PCR, total RNA (100 ng) extracted from six embryonic developmental windows was reverse transcribed in 12.5 µl with AMV RT

(Promega) according to the manufacturer's instructions in the presence of 50 ng of downstream primer, namely EX3R for *elav* coding transcript detection, EX4R for the detection of a type of non-coding transcript (RE58603) or RP49R for the control of RNA abundance. PCRs were performed on the RT products using *Taq* DNA polymerase in the presence of appropriate primer pairs: EX2F plus EX3R for the RT with EX3R, yielding a 350 bp product, EX2F plus 5599R for the RT with EX4R (5599R anneals upstream of EX4R) yielding a 269 bp product, and RP49F plus RP49R, yielding a 364 bp product. PCR products were analysed on agarose gels, and aliquots of the *elav* RT–PCR products were sequenced for verification. EX2F, CGAAGCAGAGAGCAAGGA; EX3R, GATTGCCTGTTGCACCTGT; EX4R, TCCTGTCCCACAGTGTGT; 5599R, TCCTTATATGCGGCTGCCT; RP49F, ATCGATATGCTAAGCTGT; RP49R, ACGTTACAAGAACTCTCA.

RESULTS

Iterative *in vitro* selection identifies the site preferentially bound by ELAV in the *elav* 3′-UTR

elav autoregulates through a mechanism requiring the *elav* 7 kb long 3′-UTR (36). Given the ability of ELAV to bind RNA, a plausible mechanism of regulation could rely upon direct ELAV binding to the *elav* 3′-UTR. To evaluate this possibility, we decided to identify potential binding sites in the *elav* 3′-UTR.

We performed an iterative *in vitro* selection with GST-ELAV as a target, and RNA obtained by transcription of a library representative of the *elav* 3′-UTR referred to as the OL (Figure 1 and Materials and Methods). We chose this customized approach, using as RNA targets actual genomic *Drosophila* sequences, so that we could directly identify a specific binding site rather than a consensus sequence, which can be ambiguous. A somewhat similar approach was used for iterative selection of Hel-NI (a human ELAV-like protein) binding sequences, from libraries of naturally occurring 3′-UTR sequences (39).

The progress of the enrichment was monitored (i) by shift assays, to assess the ability of given RNA populations to associate with ELAV, (ii) by Southern blot analysis of the genomic clone used to generate OL, using labelled populations of partitioned RNAs as probes, since the homogenization of the RNA population is expected to lead to simplification of the hybridization pattern and (iii) by establishment of binding curves (established by nitrocellulose filtration) between ELAV and the population of RNA, another means to evaluate the affinity of RNAs for ELAV (Figure 1). Based upon these criteria, after two cycles, a dramatic change in the partitioned RNA population profile was observed and after three additional cycles optimal enrichment was obtained (Figure 1A and B).

We cloned and sequenced 12 cDNAs made from the partitioned RNAs of the last cycle (S5 clones). Insert sizes ranged from 81 to 118 nt. Their sequences were grouped into three non-overlapping clusters (Figure 1D and E). Cluster 1 (C1, 8 of 12 sequenced clones) spans 183 nt in the 3′-UTR, with a 20 nt long overlap in region 12 331–12 350 of the *elav* 3′-UTR. Cluster 2 (C2, 2 of 12 sequenced clones) spans 103 nt, with an overlap in region 9730–9830, and an insertion leading to 12 and 15 additional units, respectively, towards the 3′ end of the RNA. Cluster 3 (C3, 2 of 12 sequenced clones) covers 109 nt with an overlap in region 11 908–11 987. The clones defining C1 and C3 encode sense 3′-UTR RNA, while those defining C2 encode antisense 3′-UTR RNA.

Shifts assays were performed with representative clones of the three cluster types, and all demonstrate significant ELAV binding (Figure 1C and data not shown for C2 clones) confirming that the partitioned RNA population was selected on the basis of its affinity for ELAV.

C1 clones appear to encode the ELAV best binding site because of their predominance. C2 clones encode artefactual antisense RNA, and we excluded it as the target we were looking for. C3 clones are significantly less represented than C1 clones in the final partitioned pool 5 (Southern hybridizations Figure 1A and C), but interestingly, in pool 2, C1 and C3 clones were both significantly represented (Figure 1A and C). Although a second independent *in vitro* partitioning did not provide evidence for enrichment of C3 type clones, but only for type C1 clones, we do not exclude the possibility that C3 clones might encode a secondary binding site for ELAV.

ELAV binding to its best binding site in the *elav* 3′-UTR is sequence specific

The C1 clones show an overlap of 20 nt (AUUUUUAUUUGUUAUUUUUU; Figure 1D), that we refer to as selected site for ELAV (SSE). By deduction, this sequence should define the ELAV best binding site. To evaluate this possibility, we examined the binding of ELAV to specific RNA targets (Figure 2C). On shift assays (Figure 2A), ELAV similarly binds SSE1F, a 120 nt long RNA including SSE, and EXS6, a 135 nt long RNA including one of the four binding sites for ELAV identified by cross-linking experiments in the *neuroglian* gene (14). It also binds SSE1FΔ, a 65 nt long truncated version of SSE1F including SSE (data not shown). In contrast, it poorly binds SSE1R, the reverse complement to SSE1F (Figure 2A). Interestingly, reproducible patterns of multiple bands are seen, indicating that several types of complexes are sequentially formed as ELAV concentration increases (Figure 2A). We established the binding curves of ELAV to the different RNA targets by nitrocellulose filtration, and found that SSE1F and EXS6 have comparable affinities for ELAV (K_d of ~40 nM), while the antisense RNA has a K_d greater than 1 μM (Figure 2B). Therefore, the 65 nt RNA containing the SSE sequence is sufficient for significant and specific ELAV binding. We further demonstrated the sequence specificity of the ELAV–RNA interaction by showing that poly(U) can compete for binding of ELAV to an SSE-containing RNA, while poly(A) has no effect (Figure 3A).

Finally, we showed that a 20mer RNA oligonucleotide corresponding to SSE also competes the binding of ELAV to SSE1F, while a mutated version of this RNA (SSE~C, mutation of the G to C) does not compete as efficiently (Figure 3B). An 8-fold excess of cold SSE~G competitor is sufficient to partially prevent binding, whereas the same excess of SSE~C has no effect. These experiments show that SSE is directly bound by ELAV and demonstrate the sequence specificity of its binding.

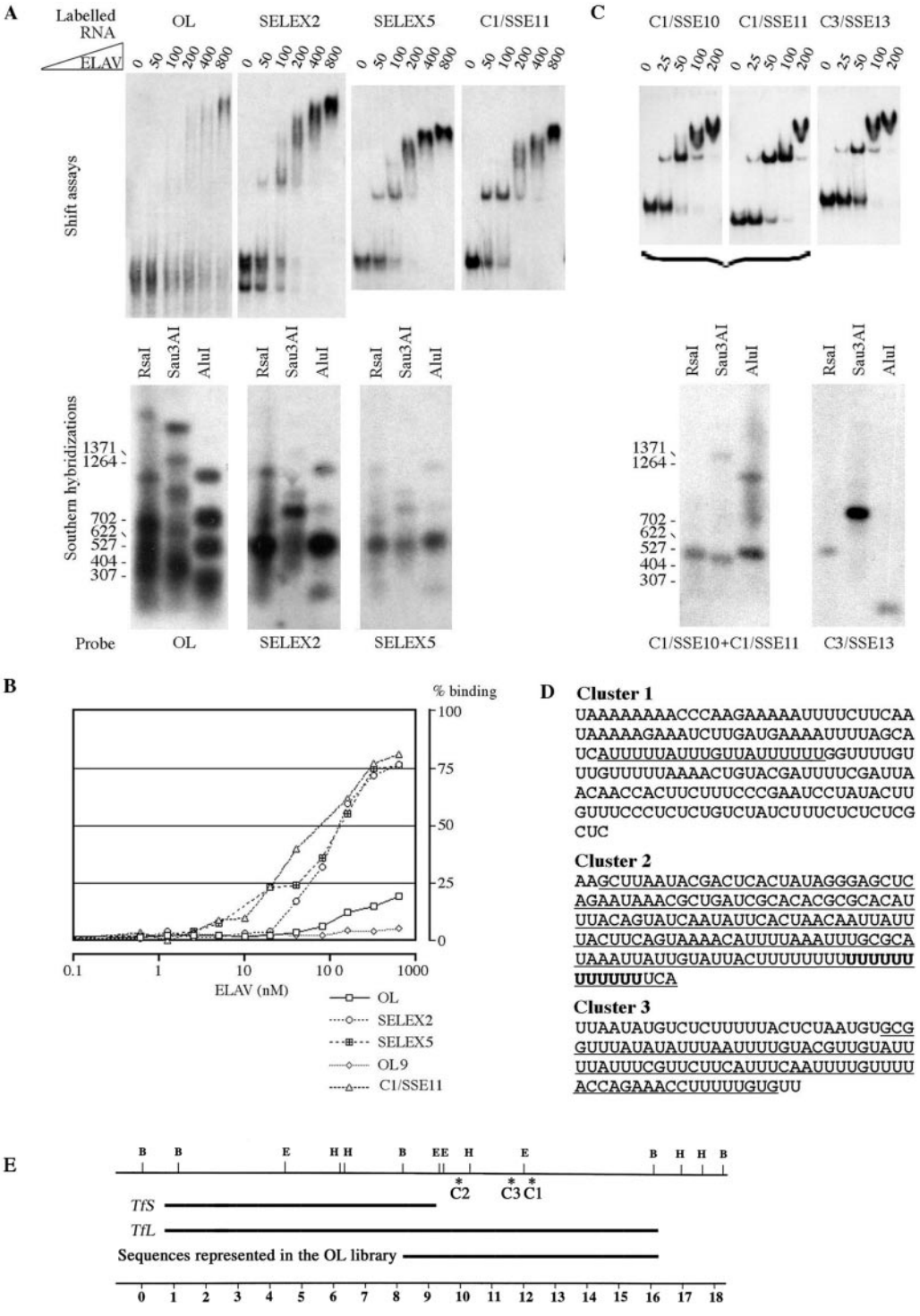

Figure 1. Selection of the ELAV best binding site. (**A**) Upper panels: labelled RNAs (1000 d.p.m., 1.5–2 nM) were used in shift assays with GST-ELAV protein, concentration in nM as indicated. The four panels are from the same experiment, run on two gels. Lower panels: Southern hybridizations to RsaI-, Sau3AI- or AluI-digested p7.5BB, covering the *elav* 3′-UTR sequence, are shown below the shifts. Molecular weight (bp) on the left. (**B**) Binding curve between GST-ELAV protein and RNA pools or discrete RNA species. All experiments were performed in parallel with the same protein batch. (**C**) Tests by shift assays and Southern hybridization of representative clones of clusters C1 and C3 which were identified through partitioning, as in (A). (**D**) Sequence covered by the three non-overlapping clusters (C1, C2 and C3). In the scale from (E), C1, coordinates 12 269–12 451; C2, coordinates 9730–9832; C3, coordinates 11 881–11 989. The sequences overlapping within each cluster are underlined and a 12 U insertion typical of C2 RNAs is bold. (**E**) Schematics of the *elav* locus (B, BamHI; E, EcoRI; H, HindIII), with a scale in kb at the bottom, as defined previously (48). Asterisks indicate the position of C1, C2 and C3. The span of the genomic fragments included in the *TfS* and *TfL* minigenes is shown. *TfS* rescue *elav* function, but only *TfL* show autoregulation of the gene. Also indicated is the region from which the OL was made. RNA symbols: OL, original library RNA pool; Pool 2, RNA pool after two partitioning cycles; Pool 5, RNA pool after five partitioning cycles; C1/SSE10 and C1/SSE11, RNAs from C1 clones, coordinates 12 270–12 350 and 12 331–12 451, respectively. C3/SSE13, RNA from a C3 clone, coordinates 11 908–11 987; OL#9, RNA from an OL clone with a 50% GC content.

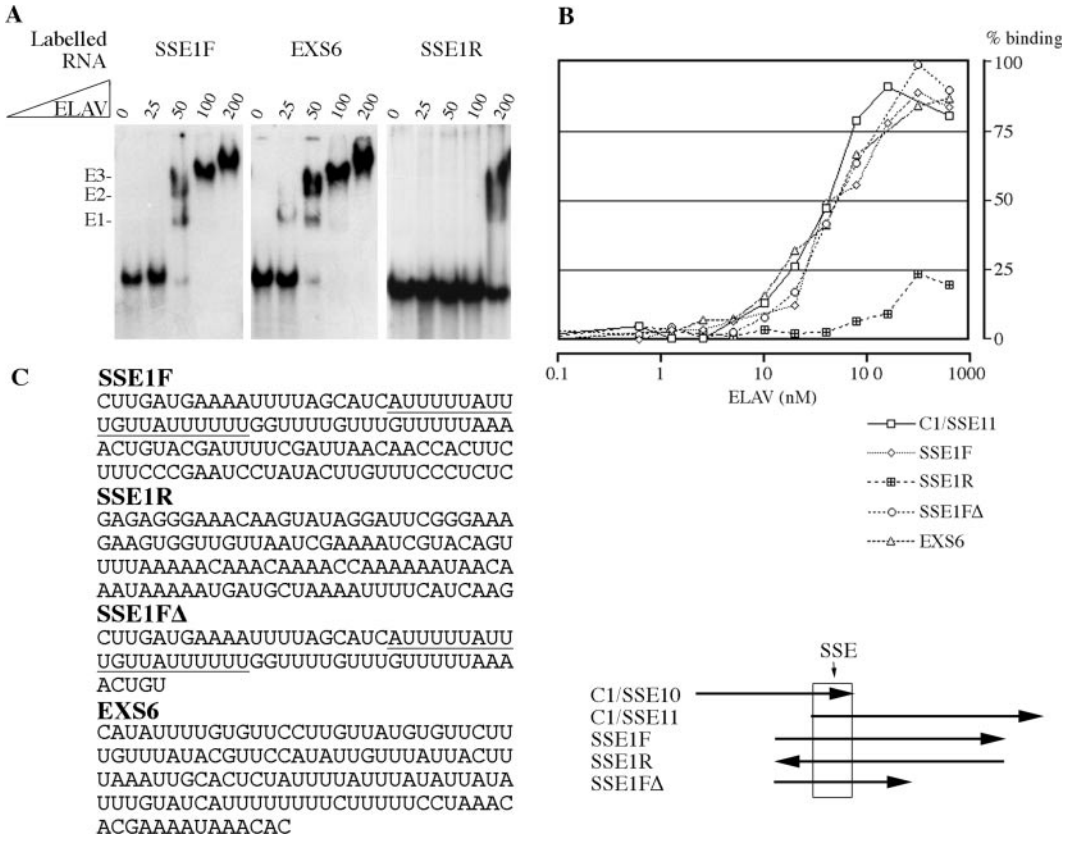

Figure 2. ELAV specifically binds discrete sequences. (**A**) Labelled RNAs (1.5–3 nM) were used in shift assays with GST-ELAV protein, concentration in nM as indicated. All panels from the same experiment. The first protein–RNA complexes formed (sequentially E1, E2 and E3) are indicated. (**B**) Binding curve between GST–ELAV protein and discrete RNA species, all experiments performed in parallel with the same protein batch. (**C**) Sequence of the target RNAs tested in Figure 2A. SSE, the region common to the RNAs from cluster 1 (Figure 1) is underlined. A diagram of the RNAs with the relative overlaps is on the right. RNA symbols and coordinates in the scale from Figure 1. SSE1F, coordinates 12 310–12 429 in *elav* 3′-UTR. SSE1R, reverse complement to SSE1F. SSE1FΔ, coordinates 12 310–12 374 in *elav* 3′-UTR. EXS6, RNA derived from a *neuroglian* intron (14). These RNAs also include sequences encoded by the plasmid, respectively, GGGCGAAUUGGGGAUU in 5′ and, except for SSE1FΔ, AUCACUAGUGC in 3′. C1/SSE10 and 11 (Figure 1).

The RRMs of ELAV have distinct RNA-binding specificities

We showed that ELAV similarly binds the *nrg* and *elav* RNA targets. To determine if recognition of a specific target is performed by specific RRM(s), we examined their binding specificity. First, we used an assay that classifies RNA-binding proteins according to their binding properties to homoribopolymers. In this assay, ELAV binds to homoribopolyuridylic acid and not to poly(A), poly(G) or poly(C), although weak binding to poly(G) is detected at low salt concentration (100 mM NaCl) (8). We tested the individual RRMs in this assay to evaluate their potential RNA-binding properties, and found that, similar to ELAV, both RRM1 and RRM3 bind poly(U) (Figure 4A and B). However, no binding was observed for RRM2. In addition, weak poly(G) binding was observed in the case of RRM1 (Figure 4B). Thus, the binding specificity of individual RRMs to homoribopolymers in this assay summarizes the specificity of ELAV essentially as a poly(U) binding protein.

To assess the specificity of the binding of the *nrg* site and the *elav* site by individual RRMs we used them in shift assays with a mixture of *elav* and *nrg* target RNAs whose sizes differ, allowing simultaneous monitoring of the binding of the two targets (Figure 4C). We found that RRM1 binds to *elav* and *nrg* targets with apparently similar affinities, since the ratio between the two RNAs remains constant. RRM3 shows an overall lower RNA affinity than RRM1 and, contrary to RRM1, exhibits a preference for the *nrg* target (Figure 4C). Again, RRM2 does not show RNA-binding activity. Although, as has been seen for other ELAV-like proteins (19) independent ELAV RRMs have a lower affinity for their RNA targets than the whole ELAV protein, their binding specificity recapitulates that of the whole protein (Figures 2 and 4), with RRM1 being the most effective individual RNA-binding domain.

FNE shares common RNA targets with ELAV

We described previously an *elav* paralogue (*fne*) whose product is concentrated in the cytoplasm of neurons, where its overexpression causes a decrease in stable *elav* transcript levels (8). Both ELAV and FNE show high affinity for polyuridylic acid, but ELAV is more versatile and also binds to single- and double-stranded DNA (8). We tested whether the interaction between the two genes could rely upon interaction of their

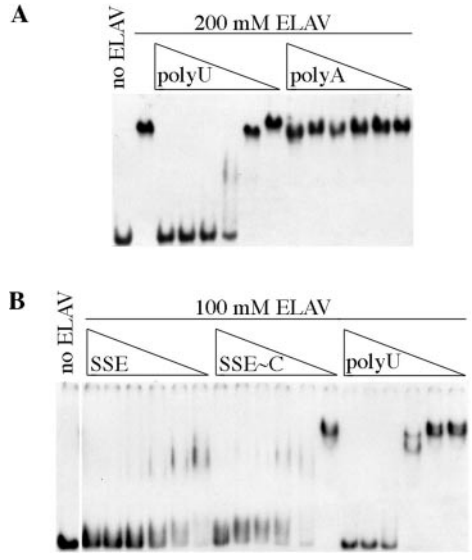

Figure 3. Competition study of ELAV binding to SSE. Shift assays with labelled SSE1F RNA (3 nM) and specific unlabelled RNA competitors. The RNAs were mixed and denatured prior to the addition of GST–ELAV (concentration as indicated). (**A**) 2-Fold dilutions of competitors [5–0.15 μg poly(U) and poly(A), average size 600mers, Sigma P9528 and P9403]: 400×, 200×, 100×, 50×, 25× and 12.5× excess molarity compared with SSE1F. (**B**) 5-Fold dilutions of competitors (10 μg to 3.2 ng). SSE, SSE∼C: 25 000×, 5000×, 1000×, 200×, 40× and 8× excess molarity compared with SSE1F, and poly(U) (as in Figure 3A): 800×, 160×, 33×, 7×, 1.3× and 0.26× excess molarity compared with SSE1F. SSE, AUUUUUAUUUGUUAUUUUUU; SSE∼C, SSE with the substitution of G by C.

protein products with the same binding site. Consistent with this possibility, shift assays show that, similarly to ELAV, FNE specifically binds to *elav* and *nrg* RNA targets (Figures 2A and 5A). Furthermore, as shown when providing *nrg* and *elav* RNA targets simultaneously in shift assays, both FNE and ELAV bind the two RNAs with apparently similar affinities (Figure 5B). As for ELAV, we observe reproducible patterns of bands presumably corresponding to sequentially formed complexes as FNE concentration increases (Figure 5A). GST–FNE7, a fusion missing the 72 N-terminal amino acids of RRM1, also shifts *elav* RNA (SSE1F) and sequential complexes visible by gel shifts are formed (data not shown).

We performed binding assays by mixing ELAV and FNE proteins to determine if RNA binding by one protein affects binding by the other. The impact of the progressive addition of ELAV on FNE–RNA interactions (Figure 5C) reveals good consistency between the intensity of the shift and the total protein concentration, with the progressive addition of ELAV causing an increased shift of the RNA, (Figures 2A, 5A and C). Thus, binding of one protein neither inhibits nor favours the binding of the other.

At high protein concentrations, high molecular weight complexes are formed (Figure 5D) We noticed that the migration of the complexes formed at equimolar ELAV and FNE concentrations (80 nM each) is intermediate to the migration of FNE–RNA complexes and ELAV–RNA complexes at 160 nM protein concentrations, respectively. This indicates that hybrid complexes including the RNA(s) and both ELAV and FNE can be formed.

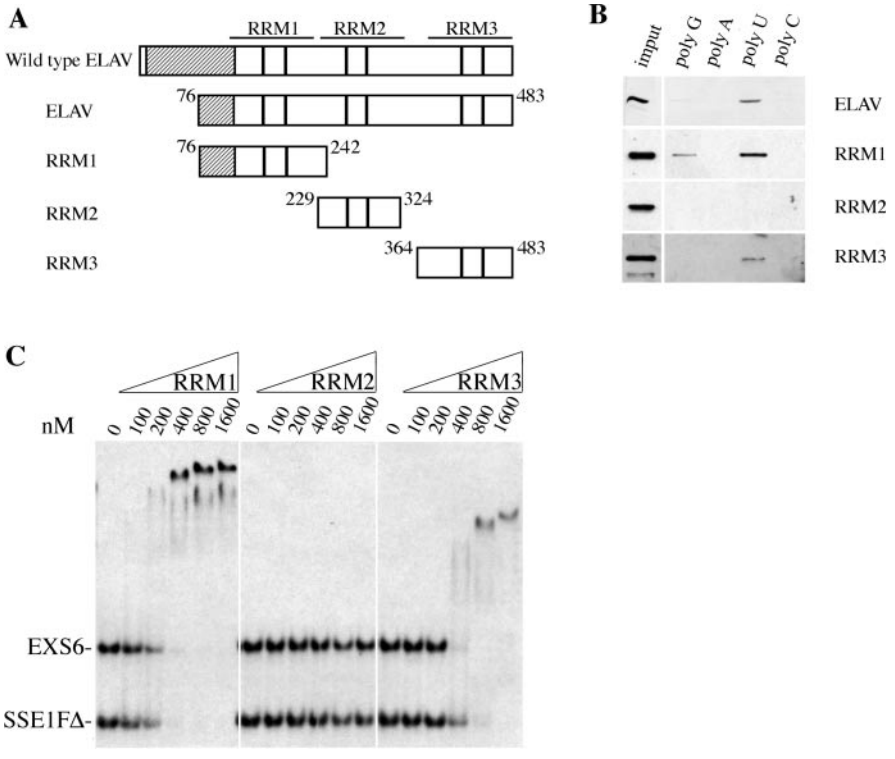

Figure 4. ELAV RRMs show distinct RNA-binding properties. (**A**) Diagram of the fusion proteins. Wild-type ELAV, full-size ELAV protein. The boxed area corresponds to the QA-rich N-terminal domain. The portions of ELAV fused downstream of the GST domain in the fusions are shown below. RRM, RNA recognition motif. The pairs of vertical bars correspond to the signature motifs RNP-CS2 and RNP-CS1. (**B**) Binding assays between GST-fusions and resin-conjugated homoribopolymers, as indicated. (**C**) Shift assays with a mixture of EXS6 and SSE1FΔ RNAs (1.5 nM each) and GST–RRM fusions (concentrations as indicated). All panels from the same experiment.

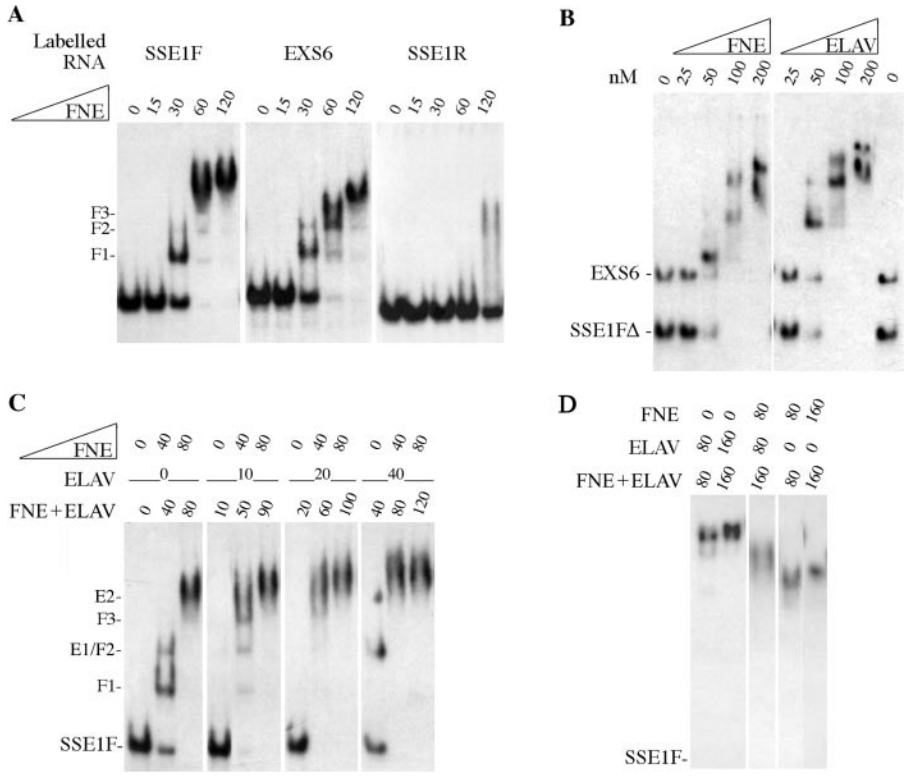

Figure 5. FNE, a protein of the ELAV family, shares common RNA targets with ELAV. (**A**) Labelled RNAs (1.5–3 nM) were used in shift assays with GST-FNE2 protein, concentration in nM as indicated. The first protein–RNA complexes formed (sequentially F1, F2 and F3) are indicated. (**B**) Shift assays with a mixture of EXS6 RNA (1.5 nM) and SSE1FΔ RNA (2.5 nM) with GST–FNE2 or GST–ELAV fusions (concentrations as indicated). (**C** and **D**) Shift assays of SSE1F RNA (3 nM) with mixtures of ELAV and FNE proteins. All panels from the same experiment.

A complex array of coding and non-coding transcripts is produced from the *elav* locus

The stable transcript pattern of *elav* is complex and dynamic, in contrast with the fact that only one form of protein is produced. Neither the gene sequence nor functional data predict the existence of alternative protein forms. It thus seems probable that the observed transcript complexity reflects *elav* post-transcriptional regulation. We have shown previously that the level of ELAV protein produced in neuron is tightly regulated and independent of gene dosage (36). We wished to determine how the binding of ELAV to the SSE-binding site in the *elav* 3′-UTR could contribute to gene regulation, and for that purpose we examined the structure of transcripts produced from the *elav* locus.

Although a complete 2.5 kb functional *elav* cDNA (cDNA-1/LD33076, Figure 6A) has been identified, all the *elav* RNA detected on northern blots with single-stranded antisense probes corresponding to cDNA-1 are larger than 5 kb (8). To gain insight into the structure of the multiple forms of *elav* RNA, we screened cDNA libraries (from *Drosophila* heads and embryos) (8). In addition, cDNAs identified by the Berkeley *Drosophila* Genome Project (38) were examined, and we completed the sequencing of those that we suspected might differ from the original coding *elav* cDNA-1 (Figure 6A).

The larger *elav* transcripts are absent as full-size cDNAs from the cDNA libraries, but partial cDNAs allow the (not necessarily exhaustive) identification of four alternative polyadenylation sites and alternative exon/intron boundaries (Figure 6A). Surprisingly, several forms of non-coding RNA exist, that we separate into two categories. First, those that differ from cDNA-1 by the exon(s), upstream of the *elav* ORF (Figure 6A), indicating that one level of regulation of *elav* expression is mediated by the regulation of the splicing event that generates the initiating ATG. Second, we identified a form of cDNA (RE58603) alternative to the coding cDNA-1, which includes an alternative non-coding 3′ terminal exon (Figure 6A). It seems that a primary transcript that matures in multiple fashions is produced from the *elav* locus. Processing results in either RNA capable of producing ELAV protein, or on the contrary on abortive RNAs, a mechanism that could be very efficient at regulating ELAV protein levels.

The ELAV best binding site in the *elav* 3′-UTR maps to a non-coding alternative exon

ELAV binds to a site, SSE, retained in RE58603 (Figure 6A). This non-coding RE58603 cDNA differs from the coding cDNA-1 by the substitution of a non-coding 3′ exon that replaces the 3′ coding 3′ exon of cDNA-1. This suggests a simple model, whereby when ELAV levels pass a given threshold, the protein binds to its own 3′-UTR (at SSE) in the pre-mRNA, favouring the generation/accumulation of non-coding RNA (RE58603) versus that of a coding RNA (LD33076).

To test this hypothesis, we first determined by northern blot the pattern of expression of RNAs including the third exon

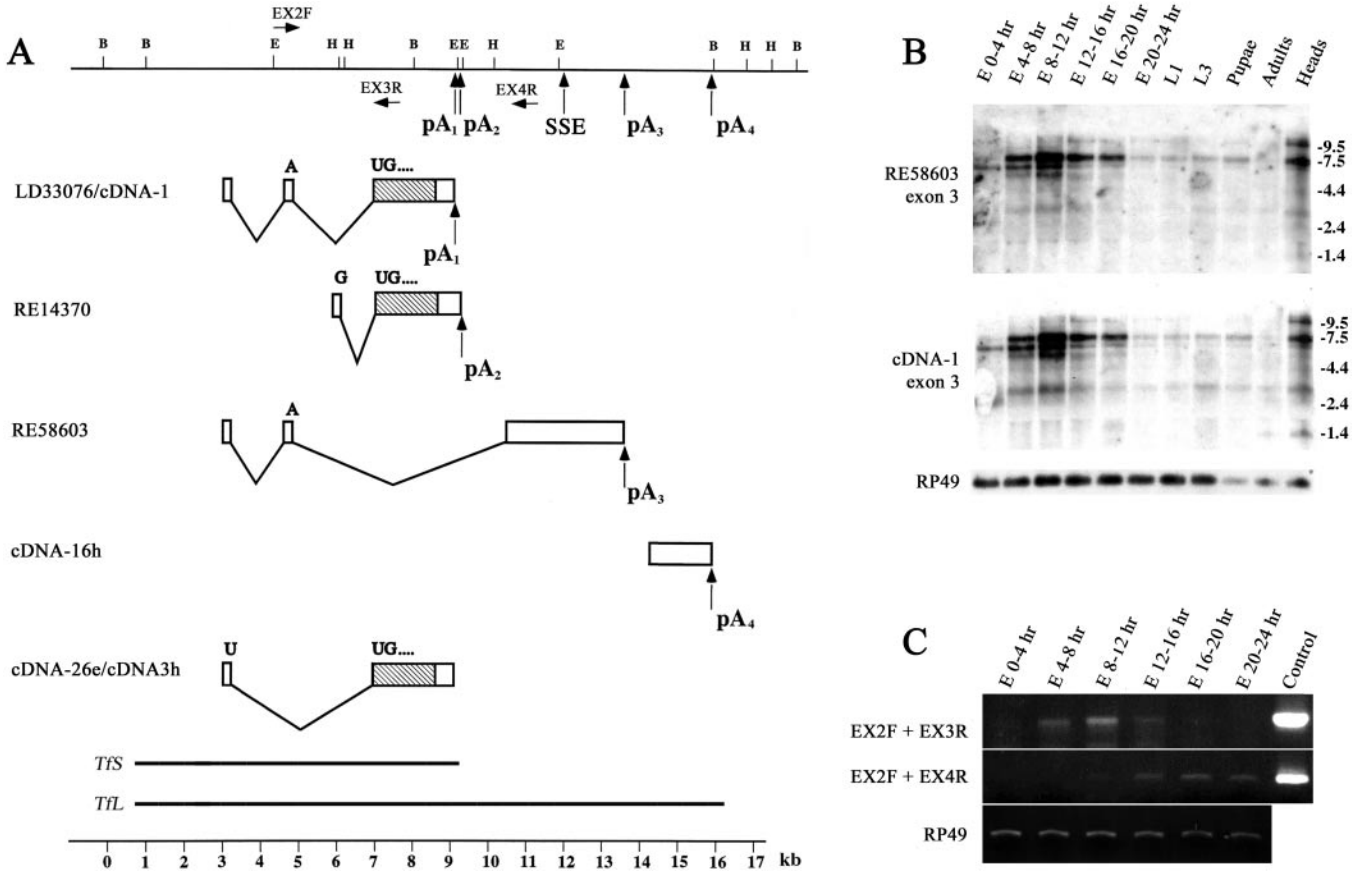

Figure 6. Alternative polyadenylation and splicing at the *elav* locus. (**A**) The locus is shown as a continuous line (B, BamHI; E, EcoRI; H, HindIII), with a scale in kb at the bottom of (A), as in Figure 1. The *elav* ORF is shown as a striped box (except for the A of the initiator codon) starting at nt 7099 and finishing at 8549. *TfS* and *TfL* as in Figure 1. The structure of *elav* mRNAs, derived from the complete sequencing of cDNA clones, is indicated. All cDNAs were obtained from embryonic libraries, except for cDNA-16h and cDNA3h which were from adult head libraries. All four polyadenylation sites (pA) are included in the previously reported *TfL* minigenes, which are expressed normally (36). Only the most 5′ poly(A) site is included in *TfS* minigenes that are able to provide *elav* function but are mis-regulated (36). Similar to the *TfS* minigenes, LD33076/cDNA-1 is sufficient to rescue *elav* null function completely when under the control of *elav* 5′-UTR sequences and a 3′ tubulin trailer, but it is mis-regulated (36). Note that the coding cDNA LD33076 includes a 54 A long poly(A) tail and uses the pA1 polyadenylation site. Its structure is identical to that of cDNA1 which has been hypothesized previously to possess a truncated 3′ end because of (i) its size discrepancy with the *elav* stable transcripts detected on northern blots and (ii) the knowledge that *elav* transcripts extended downstream. The position of the SSE *elav*-binding site and the primers EX2F, EX3R and EX4R used in the RT–PCR experiments of (C) are indicated. (**B**) Developmental analysis of *elav* transcripts. The filter was first hybridized with an antisense probe corresponding to exon 3 of RE58603 (upper panel) and then re-hybridized with a probe corresponding to exon 3 of cDNA-1 (lower panel), and finally to an antisense RP49 probe as a loading control. An antisense probe corresponding to the incomplete adult cDNA-16h (between pA3 and pA4) does not detect any RNA on northern blots, but it detects the central nervous system of embryos by *in situ* hybridization (data not shown), as expected for an *elav* transcript. Molecular weights on the right. E, embryonic stages with the window of development specified; L1 and L3, first and third instar larvae, respectively. (**C**) RT–PCR for the detection of coding transcripts (EX2F plus EX3R primers, Figure 6A), alternative non-coding trancripts of the RE58603 type, (EX2F plus EX4R primers, Figure 6A), and RP49 used as a control for RNA abundance. Windows of embryonic development as indicated. The control lane shows the PCR products obtained by amplification of cDNA clones: cDNA-1 in the case of EX2F plus EX3R primers, and RE58603 in the case of EX2F plus EX4R.

of the non-coding cDNA RE58603 (between pA2 and pA3, Figure 6A) in the *elav* RNAs. Surprisingly, most of these RNAs are the same as those detected by an antisense *elav* ORF probe, although the 3 kb RNA corresponding to RE58603 itself is not detected (Figure 6B). Clearly, complex transcripts that were not identified as full-size cDNA clones and that include large portions of the *elav* locus are produced, making it impossible to distinguish between the RNA with a coding exon 3 and a proper ATG (type cDNA-1) versus its non-coding counterpart including a non-coding alternative exon 3 (type LD33076).

We thus reasoned that all the functional *elav* RNA, including hypothetical forms that would differ from the cDNA-1 type by including, for instance, an extended 3′-UTR, must share the common splicing event that generates the ATG initiation codon. We identified these by RT–PCR using the EX2F and EX3R primers, in parallel with the alternative non-coding transcript of the RE58603 type, that were detected with the EX2F and EX4R pair of primers (Figure 6A and C). As predicted by our model, the coding transcript accumulates from the time neurons start to be born (∼5 h of development) and peaks ∼8–12 h of development, shortly before the birth of the last embryonic neurons. In contrast, non-coding transcripts first appear coincidentally with the peak of the coding transcript (8–12 h). Their level rises and plateaus until the end of embryonic development.

DISCUSSION

ELAV binds a site in the *elav* 3′-UTR that resembles binding sites already identified in *nrg* and *ewg*

ELAV-binding sites have been reported in regulated introns of *nrg* and *erect wing* (*ewg*) (14,16). In *nrg* RNA, they are defined as long tracts including at least two 8–10 nt-long U-rich stretches. In *ewg* RNA, ELAV-binding sites consist of AU-rich elements including three to four tandemly repeated $A(U_{4-6})$ sequences. Our approach allowed us to map the ELAV best binding site in its RNA to a shorter U-rich sequence that is only 20 nt long (SSE). We found that the affinity of ELAV for a 65 nt long RNA including SSE is in the nanomolar range, similar to that of ELAV for a 164 nt long RNA derived from *ewg* proposed to bind several ELAV molecules (16). It is also similar to ELAV affinity for an RNA including the 114 nt long EXS6 from *nrg* RNA that cross-links to ELAV (this paper).

Competition experiments highlight the higher affinity of ELAV for the SSE site than for a mutant version of the site where a C replaces the single G. Thus, the interaction between ELAV and the RNA depends in part upon recognition of specific bases, not just of the phosphate sugar-backbone.

Sequence analysis of 500 nt framing SSE with the Stem Loop program as well as attempts to identify secondary structures with the programs Mfold and PlotFold (GCG Wisconsin Package) in the 65 nt long SSE1FΔ RNA failed to identify any secondary structure with base pairing of SSE (data not shown). ELAV thus binds ssRNA, reminiscent of the binding of the SXL and HuD proteins, whose two RRMs share extensive structural similarity with ELAV RRM1 and RRM2 and which also bind ssRNA with no base pairing (23,24).

An ELAV-binding site with a U-rich sequence and a low dissociation constant with ELAV was thus identified in the *elav* 3′-UTR. The characteristics of this site resemble those of the previously identified ELAV targets, supporting the validity of the binding site that we identified in the *elav* 3′-UTR, and thus our model that *elav* autoregulation depends upon direct binding of ELAV to the 3′-UTR of *elav* RNA.

ELAV RRM1 and RRM3 bind RNA on their own with different specificities

ELAV protein and its homologues contain three conserved RNA-binding domains. Mutations in any of the three domains abolish ELAV function. However domain swap experiments (with RRMs from the *Drosophila* paralogue RBP9, the *Drosophila* relative SXL or the human orthologue HuD) showed that chimeric ELAV proteins with substituted RRM3, but not RRM1 and/or RRM2, are functional (40).

We evaluated the binding properties of individual RRMs to determine if distinct RRMs are responsible for the specific target recognition of *nrg* and *elav*-binding sites. We found that both RRM1 and RRM3 are capable of significantly binding RNA on their own, with RRM1 showing a higher affinity than RRM3. No RNA-binding activity was detected for RRM2 with the targets that we tested (*nrg*, *elav* sites, this paper; and the OL RNA, data not shown), even using different batches of proteins. We cannot exclude the possibility that the ELAV–RRM2 fusion protein, in spite of the fact that it is abundantly and stably produced, may be non-functional, possibly owing to altered folding. Another alternative is that ELAV–RRM2 can bind RNA only when another partner RRM is available, as in the case of HuD or HuC, whose second RRMs increases the affinity of RRM1 for an AU-rich sequence and stabilizes the complex (21,26).

Conserved residues between HuD and SXL interact with different bases in their different targets [U(A/U)UUUAUUUU for HuD and UGUUUUUUUUU for SXL] (23), and it thus seems possible that the same ELAV RRMs are involved in *nrg* and *elav* target recognition. However, our binding assay involving one protein and two binding sites shows that RRM1 and RRM3 display different relative affinities for the *nrg* and *elav* RNA-binding sites. As a correlate, if the properties of individual RRMs are maintained in the complete protein, ELAV binding with specific RNAs may rely upon particular interactions with different RRMs. *In vivo*, it is conceivable that the complexes might interact with different sets of factors and thus enter distinct pathways of post-transcriptional processing, depending upon which RRM is involved in RNA contact (see below).

ELAV and FNE

The neuronal protein FNE is encoded by an *elav* paralogue, and the expression of the two genes is interconnected. In particular *fne* over-expression causes a decrease of *elav* (and *fne*) stable trancript levels, suggesting feedback regulation (8). We showed that FNE and ELAV both can bind the *elav* SSE-binding site independently, and it has been shown that the two proteins can interact directly, since they have been identified in a large-scale two-hybrid screen of *Drosophila* proteins as high confidence partners (42). These two properties could be involved in the feedback regulation. FNE could regulate *elav* by binding to *elav* RNA directly or FNE could titrate ELAV, both antagonizing the occupation of RNA-binding sites by ELAV. This would require that ELAV, which is predominantly nuclear, and FNE, which is predominantly cytoplasmic, would be present in the same cellular compartment, at least transiently. HuR, an apparently nuclear human orthologue of ELAV shuttles between the nucleus and the cytoplasm (41).

We observed that, when mixing FNE and ELAV with RNA, binding complexes with RNA including both ELAV and FNE are formed. One explanation for this observation is that a low affinity-binding site is also present in the RNA target and bound at high protein concentrations, allowing bridging of protein complexes via the RNA. But, since the proteins interact directly (42), it seems more probable to us that direct protein–protein interaction, before or after RNA binding, is responsible for the formation of these complexes.

The ELAV best binding site in the *elav* 3′-UTR maps to a non-coding alternative exon

The processes required for the generation of mature mRNAs are intimately linked [reviewed in (43,44)] and depend upon *cis*-regulatory regions scattered over the entire length of an RNA. Our analysis of *elav* cDNAs provides some insights into the remarkable complexity of the transcripts, presumably reflecting post-transcriptional regulation.

The locus produces multiple abundant and/or stable transcripts whose size far exceeds that of the only coding *elav* RNA so far identified. Such a situation was first reported in the case of the gene *suppressor of white apricot*, which encodes an SR-like protein, and produces mature short transcripts that are detected only briefly during development, while larger polyadenylated unspliced RNAs are the only detected transcripts during most of development (45).

In addition, four polyadenylation sites were identified in *elav*, as was reported for some of the vertebrate Hu loci, where they have been proposed to play specific roles in post-transcriptional regulation (46). Indeed, this type of organization in the 3′ end of transcripts is not rare, since 28.6% of 8700 analysed human 3′-UTRs contain two to four polyadenylation sites (47).

Although a model where ELAV binding in the proximity of polyadenylation sites and slowing the recruitment of cleavage factors or of poly(A) polymerase can explain the data reported in the case of *nrg* and *ewg* (14,16), it does not fit in the case of the *elav* gene. The sequences of ELAV-binding sites are not dramatically different, but they differ in their nature. ELAV binding to *nrg* and *ewg* RNAs occurs in alternative 3′ introns and is responsible for the generation of alternative forms of proteins, while binding to *elav* RNA occurs in an alternative non-coding 3′ exon and does not cause protein diversity. The SXL protein, whose two RRMs share extensive structural similarity with ELAV also possesses several distinct functions, in this case at the level of splicing and of translation regulation.

We showed here that ELAV binds to a site retained in a non-coding *elav* RNA (RE58603), that differs by the inclusion of an alternate 3′-terminal exon from the functional form of *elav* mRNA (LD33076). Our RT–PCR data are in agreement with our proposed model hypothesizing that the coding transcript is produced as long as the level of ELAV protein remains below a given threshold and thus unbound to SSE. The non-coding transcript is alternatively produced by alternative choice of the terminal exon/polyadenylation site once ELAV protein level passes this threshold and binds SSE. This model provides a mechanism for the regulation of ELAV protein level, which we have genetically shown to be critical and dependent upon the *elav* 3′-UTR (36).

The dual RNA-binding mechanism, suggested by the specific preferences for different RNAs by individual RRMs, might be linked to dual functional properties, for instance via association with different additional partner proteins, which might include FNE. Future work will aim to examine this possibility in order to identify the mechanism(s), such as regulation of exon definition and/or cleavage/polyadenylation responsible for *elav* regulatory functions.

ACKNOWLEDGEMENTS

We thank Jin-Feng Wang for detailed advice on *in vitro* selection, and Leonard Rabinow for his constructive comments. We also thank Nandor Roczo for critical reading of the manuscript. This work was supported by a Basic Research Grant from the March of Dimes Birth Defects Foundation (1-FY96-0995/1-FY97-0605) to M.-L.S. in addition to funding from the Centre National de la Recherche Scientifique and the University of Paris Sud. The Open Access publication charges for this article were waived by Oxford University Press.

Conflict of interest statement. None declared.

REFERENCES

1. Yao,K.M., Samson,M.L., Reeves,R. and White,K. (1993) Gene *elav* of *Drosophila melanogaster*: a prototype for neuronal-specific RNA binding protein gene family that is conserved in flies and humans. *J. Neurobiol.*, **24**, 723–739.
2. Fribourg,S., Gatfield,D., Izaurralde,E. and Conti,E. (2003) A novel mode of RBD-protein recognition in the Y14–Mago complex. *Nature Struct. Biol.*, **10**, 433–439.
3. Shi,H. and Xu,R.-M. (2003) Crystal structure of the *Drosophila* Mago nashi–Y14 complex. *Genes Dev.*, **17**, 971–976.
4. DeAngelo,D.J., DeFalco,J., Rybacki,L. and Childs,G. (1995) The embryonic enhancer-binding protein SSAP contains a novel DNA-binding domain which has homology to several RNA-binding proteins. *Mol. Cell. Biol.*, **15**, 1254–1264.
5. Robinow,S., Campos,A.R., Yao,K.M. and White,K. (1988) The *elav* gene product of *Drosophila*, required in neurons, has three RNA consensus motifs. *Science*, **242**, 1570–1572.
6. Kim,Y.J. and Baker,B.S. (1993) The *Drosophila* gene rbp9 encodes a protein that is a member of a conserved group of putative RNA binding proteins that are nervous system-specific in both flies and humans. *J. Neurosci.*, **14**, 1943–1952.
7. Kim-Ha,J., Kim,J. and Kim,Y.-J. (1999) Requirement of RBP9, a *Drosophila* Hu homolog, for regulation of cystocyte differentiation and oocyte determination during oogenesis. *Mol. Cell. Biol.*, **19**, 2505–2514.
8. Samson,M.-L. and Chalvet,F. (2003) *Found in neurons*, a third member of the *Drosophila elav* gene family, encodes a neuronal protein and interacts with *elav*. *Mech. Dev.*, **120**, 373–383.
9. Ma,W.J., Cheng,S., Campbell,C., Wright,A. and Furneaux,H. (1996) Cloning and characterization of HuR, a ubiquitously expressed Elav-like protein. *J. Biol. Chem.*, **271**, 8144–8151.
10. Wakamatsu,Y. and Weston,J. (1997) Sequential expression and role of Hu RNA-binding proteins during neurogenesis. *Development*, **124**, 3449–3460.
11. Pascale,A., Gusev,P.A., Amadio,M., Dottorini,T., Govoni,S., Alkon,D.L. and Quattrone,A. (2004) Increase of the RNA-binding protein HuD and posttranscriptional up-regulation of the GAP-43 gene during spatial memory. *Proc. Natl Acad. Sci. USA*, **101**, 1217–1222.
12. Quattrone,A., Pascale,A., Nogues,X., Zhao,W., Gusev,P., Pacini,A. and Alkon,D. (2001) Posttranscriptional regulation of gene expression in learning by the neuronal ELAV-like mRNA-stabilizing proteins. *Proc. Natl Acad. Sci. USA*, **98**, 11668–11673.
13. Park,S.J., Yang,Y.E., Kim-Ha,J. and Kim,Y.-Y. (1998) Down regulation of extramacrochaetae mRNA by a drosophila neural RNA binding protein Rbp9 which is homologous to human Hu proteins. *Nucleic Acids Res.*, **26**, 2989–2994.
14. Lisbin,M.J., Qiu,J. and White,K. (2001) The neuron-specific RNA binding protein ELAV regulates neuroglian alternative splicing in neurons and binds directly to its pre-mRNA. *Genes Dev.*, **15**, 2546–2561.
15. López de Silanes,I., Zhan,M., Lal,A., Yang,X. and Gorospe,M. (2004) Identification of a target RNA motif for RNA-binding protein HuR. *Proc. Natl Acad. Sci. USA*, **101**, 2987–2992.
16. Soller,M. and White,K. (2003) ELAV inhibits 3′-end processing to promote neural splicing of *ewg* pre-mRNA. *Genes Dev.*, **17**, 2526–2538.
17. Myer,V.E., Fan,X.C. and Steitz,J.A. (1997) Identification of HuR as a protein implicated in AUUUA-mediated mRNA decay. *EMBO J.*, **16**, 2130–2139.
18. Park-Lee,S., Kim,S. and Laird-Offringa,I.A. (2003) Characterization of the interaction between neuronal RNA-binding protein HuD and AU-rich RNA. *J. Biol. Chem.*, **41**, 39801–39808.
19. Chung,S., Jiang,L., Cheng,S. and Furneaux,H. (1996) Purification and properties of HuD, a neuronal RNA-binding protein. *J. Biol. Chem.*, **271**, 11518–11524.
20. Levine,T.D., Gao,F., King,P.H., Andrews,L.G. and Keene,J.D. (1993) Hel-N1: an autoimmune RNA-binding protein with specificity for 3′ uridylate-rich untranslated regions of growth factor mRNAs. *Mol. Cell. Biol.*, **13**, 3494–3504.

21. Abe,R., Sakashita,E., Yamamoto,K. and Sakamoto,H. (1996) Two different RNA binding activities for the AU-rich element and the poly(A) sequence of the mouse neuronal protein mHuC. *Nucleic Acids Res*., **24**, 4895–4901.
22. Ma,W.-J., Chung,S. and Furneaux,H. (1997) The Elav-like proteins bind to AU-rich elements and to the poly(A) tail of mRNA. *Nucleic Acids Res*., **25**, 3564–3569.
23. Wang,X. and Tanaka Hall,T.M. (2001) Structural basis for recognition of AU-rich element RNA by the HuD protein. *Nature Struct. Biol*., **8**, 141–145.
24. Handa,N., Nureki,O., Kurimoto,K., Kim,I., Sakamoto,H., Shimura,Y., Muto,Y. and Yokoyama,S. (1999) Structural basis for recognition of the *tra* mRNA precursor by the Sex-lethal protein. *Nature*, **398**, 579–585.
25. Antson,A.A. (2000) Single stranded RNA binding proteins. *Curr. Opin. Struc. Biol*., **10**, 87–94.
26. Park,S., Myszka,D.G., Yu,M., Littler,S.J. and Laird-Offringa,I.A. (2000) HuD RNA recognition motifs play distinct roles in the formation of a stable complex with AU-rich RNA. *Mol. Cell. Biol*., **20**, 4765–4772.
27. Kanaar,R., Lee,A.L., Rudner,D.Z., Wemmer,D.E. and Rio,D.C. (1995) Interaction of the sex-lethal RNA-binding domains with RNA. *EMBO J*., **14**, 4530–4539.
28. Antic,D., Lu,N. and Keene,J.D. (1999) ELAV tumor antigen, Hel-N1, increases translation of neurofilament M mRNA and induces formation of neurites in human teratocarcinoma cells. *Genes Dev*., **13**, 449–461.
29. Manohar,C.F., Short,M.L., Nguyen,A., Nguyen,N.N., Chagnovich,D., Yang,Q. and Cohn,S.L. (2001) HuD, a neuronal-specific RNA-binding protein, increases the *in vivo* stability of MYCN RNA. *J. Biol. Chem*., **277**, 1967–1973.
30. Gallouzi,I.E. and Steitz,J.A. (2001) Delineation of mRNA export pathways by the use of cell-permeable peptides. *Science*, **294**, 1895–1901.
31. Fan,X.C. and Steitz,J.A. (1998) Overexpression of HuR, a nuclear cytoplasmic shuttling protein, increases the *in vivo* stability of ARE-containing mRNAs. *EMBO J*., **17**, 3448–3460.
32. Peng,S.S.-Y., Chen,C.-Y.A., Xu,N. and Shyu,A.-B. (1998) RNA stabilization by the AU-rich element binding protein, HuR, an ELAV protein. *EMBO J*., **17**, 3461–3470.
33. Kullman,M., Gopfert,U., Siewe,B. and Hengst,L. (2002) ELAV/Hu proteins inhibit p27 translation via an IRES element in the p27 5′ UTR. *Genes Dev*., **16**, 3087–3099.
34. Koushika,S.P., Lisbin,M.J. and White,K. (1996) ELAV, a *Drosophila* neuron-specific protein, mediates the generation of an alternatively spliced neural protein isoform. *Curr. Biol*., **6**, 1634–1641.
35. Koushika,S.P., Soller,M. and White,K. (2000) The neuron-enriched splicing pattern of *Drosophila* ercet wing is dependent on the presence of ELAV protein. *Mol. Cell. Biol*., **20**, 1836–1845.
36. Samson,M.-L. (1998) Evidence for 3′ untranslated region-dependent autoregulation of the *Drosophila* gene encoding the neuronal nuclear RNA-binding protein ELAV. *Genetics*, **150**, 723–733.
37. Fritzwater,T. and Polisky,B. (1996) A SELEX primer. In Abelson,J. (ed.), *Combinatorial Chemistry*. Academic Press, San Diego, CA, USA, Vol. 267, pp. 275–301.
38. Rubin,G.M., Hong,L., Brokstein,P., Evans-Holm,M., Frise,E., Stapleton,M. and Harvey,D.A. (2000) A *Drosophila* complementary DNA resource. *Science*, **287**, 2222–2224.
39. Gao,F.B., Carson,C.C., Levine,T. and Keene,J.D. (1994) Selection of a subset of mRNAs from combinatorial 3′ untranslated region libraries using neuronal RNA-binding protein Hel-N1. *Proc. Natl Acad. Sci. USA*, **91**, 11207–11211.
40. Lisbin,M.J., Gordon,M., Yannoni,Y.M. and White,K. (2000) Function of RRM domains of *Drosophila melanogaster* ELAV: RNP1 mutations and RRM domain replacements with ELAV family protein and SXL. *Genetics*, **155**, 1789–1798.
41. Atasoy,U., Warson,J., Patel,D. and Keene,J. (1998) ELAV protein HuA (HuR) can redistribute between nucleus and cytoplasm and is upregulated during serum stimulation and T cell activation. *J. Cell Sci*., **111**, 3145–3156.
42. Giot,L., Bader,J.S., Brouwer,C., Chaudhuri,A., Kuang,B., Li,Y., Hao,Y.L., Ooi,C.E., Godwin,B., Vitols,E. *et al.* (2003) A protein interaction map of *Drosophila melanogaster*. *Science*, **302**, 1727–1736.
43. Reed,R. (2003) Coupling transcription, splicing and mRNA export. *Curr. Opin Cell Biol*., **15**, 326–331.
44. Proudfoot,N. (2004) New perspectives on connecting messenger RNA 3′ end formation to transcription. *Curr. Opin. Cell Biol*., **16**, 272–278.
45. Chou,T.B., Zachar,Z. and Bingham,P.M. (1987) Developmental expression of a regulatory gene is programmed at the level of splicing. *EMBO J*., **6**, 4095–4104.
46. Okano,H.J. and Darnell,R.B. (1997) A hierarchy of Hu RNA binding proteins in developing and adult neurons. *J Neurosci*., **17**, 3024–3037.
47. Beaudoing,E., Freier,S., Wyatt,J.R., Claverie,J.-M. and Gautheret,D. (2000) Patterns of variant polyadenylation signal usage in human genes. *Genome Res*., **10**, 1001–1010.
48. Samson,M.-L. (2000) *Drosophila* arginase is produced from a nonvital gene that contains the *elav* locus within its third intron. *J. Biol. Chem*., **275**, 31107–31114.